frontiers | Frontiers in Physics

ORIGINAL RESEARCH
published: 25 April 2022
doi: 10.3389/fphy.2022.894115

Nonreciprocal Waveguide-QED for Spinning Cavities with Multiple Coupling Points

Wenxiao Liu[1], *Yafen Lin*[2], *Jiaqi Li*[2] *and Xin Wang*[2]*

[1]Department of Physics and Electronics, North China University of Water Resources and Electric Power, Zhengzhou, China, [2]Institute of Theoretical Physics, School of Physics, Xi'an Jiaotong University, Xi'an, China

We investigate chiral emission and the single-photon scattering of spinning cavities coupled to a meandering waveguide at multiple coupling points. It is shown that nonreciprocal photon transmissions occur in the cavities-waveguide system, which stems from interference effects among different coupling points, and frequency shifts induced by the Sagnac effect. The nonlocal interference is akin to the mechanism in giant atoms. In the single-cavity setup, by optimizing the spinning velocity and number of coupling points, the chiral factor can approach 1, and the chiral direction can be freely switched. Moreover, destructive interference gives rise to the complete photon transmission in one direction over the whole optical frequency band, with no analogy in other quantum setups. In the multiple-cavity system, we also investigate the photon transport properties. The results indicate a directional information flow between different nodes. Our proposal provides a novel way to achieve quantum nonreciprocal devices, which can be applied in large-scale quantum chiral networks with optical waveguides.

Keywords: chiral emission, nonreciporal transmission, quantum interference, spinning cavity, waveguide-QED

OPEN ACCESS

Edited by:
Zhihai Wang,
Northeast Normal University, China

Reviewed by:
Yan Zhang,
Northeast Normal University, China
Wenzhi Jia,
Southwest Jiaotong University, China

***Correspondence:**
Xin Wang
wangxin.phy@xjtu.edu.cn

Specialty section:
This article was submitted to Optics and Photonics, a section of the journal Frontiers in Physics

Received: *11 March 2022*
Accepted: *25 March 2022*
Published: *25 April 2022*

Citation:
Liu W, Lin Y, Li J and Wang X (2022) Nonreciprocal Waveguide-QED for Spinning Cavities with Multiple Coupling Points. Front. Phys. 10:894115. doi: 10.3389/fphy.2022.894115

1 INTRODUCTION

Waveguide quantum electrodynamics (QED) has emerged as an excellent platform for studying the interactions between atoms and itinerant photons in the past 2 decades [1–3]. A one-dimensional waveguide supports a continuum of photon modes with a strong transverse confinement, and is applicable to significantly enhance light-matter interactions [3]. Moreover, waveguide-QED systems serve as quantum channels in quantum networks, which can be realized in both natural and artificial systems, such as trapped atoms (quantum dots) interacting with nanofibers [4–8] and superconducting qubits coupled with transmission lines [9–11]. To date, a great deal of quantum optical effects have been revealed in waveguide-QED systems, including controlling single-photon scattering [12–16], photon-mediated long-range interactions [17–20] and directional photon emission [21, 22].

In traditional waveguide QED, atoms are commonly considered as point-like dipoles and coupled to the waveguide at a single point. However, an emergent class of artificial atoms, called giant atoms, break down this dipole approximation. Their sizes are comparable to the wavelength of photons (phonons) interacted [23–35]. Recent experiments have demonstrated that superconducting artificial atoms can be successfully coupled with propagating surface acoustic waves at several points [36–38]. The self-interference effects among multiple points dramatically modify the emission behaviors of giant atoms, such as frequency-dependent decay rates [23, 24], decoherence-free dipole-dipole interactions [25, 26], and nonreciprocal photon transport [30, 31]. All the above achievements indicate potential applications in quantum information processing.

Optical nonreciprocity allows photons to pass through from one side but blocks it from the opposite direction, which is requisite for preventing the information back flow in quantum network. At optical frequencies, magneto-optical Faraday effect is often applied to achieve optical nonreciprocity, which is lossy and cannot be integrated effectively on a chip [39, 40]. Therefore, several magnetic-free nonreciprocal proposals were developed. Their mechanisms include optical nonlinearity [41, 42], dynamic spatiotemporal modulation [43–45], and atomic reservoir engineering [46]. Recently, the whispering-gallery-mode resonators with mechanical rotation provide another approach to study many quantum nonreciprocal phenomena [47–50]. The simplest implementation contains a spinning resonator and a stationary tapered fiber. The rotation leads to Sagnac effect and shifts the frequency of the optical mode. Compared with previous studies, the nonreciprocal transmission of light has been achieved in experiment with very high isolation (about 99.6%) [51]. In early studies, spinning resonators, similar to small atoms, typically couple to waveguides at a single point. Nevertheless, multiple-point coupling in spinning resonator-waveguide systems has not been considered, and the photon emission and transport properties in this system are worth being explored.

In this work, we address this issue by considering spinning resonators interacting with a meandering waveguide at multiple coupling points. Such resonators are akin to the "giant atoms," but with mechanical rotation. First, in the single-cavity setup, the complete unidirectional transparency over the whole optical frequency band is observed, which can be realized by considering the spinning resonator and multiple-point coupling simultaneously, with no analogy in other quantum setups. This phenomenon results from the interference effects among different coupling points and mode frequency shifts led by the Sagnac effect. Additionally, the chiral emission direction is switchable by simply changing the rotation direction and speed. Afterward, we extend to two-cavity system, where each resonator interacts with two separate points. The phase factors and the coupling strengths between the CW and CCW modes can significantly modulate the nonreciprocal transmission behaviors, which implies chiral photon transfer among different points. Employing spinning resonators as quantum nodes, those results obtained in this paper might have potential applications in large-scale chiral quantum networks.

The paper is organized as follows: in **Section 2**, we present the single-spinning-resonator model and give the motional equations. The chiral emission and nonreciprocal transmission by tuning spinning velocity or number of coupling points are also discussed. In **Section 3**, we extend to two separate spinning resonators interacting with several coupling points. Both analytical and numerical results for the weak-field transmission are obtained. Finally, the conclusions are given in **Section 4**.

2 A SPINNING RESONATOR INTERACTING WITH MULTIPLE POINTS

2.1 Hamilton and Motional Equations

Here we first consider a spinning optical resonator evanescently coupled to a meandering optical waveguide at N coupling points,

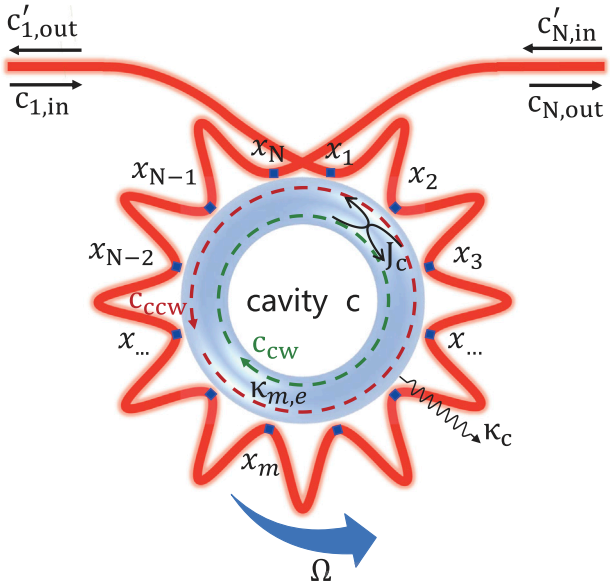

FIGURE 1 | (Color online) Schematic of a spinning resonator coupled to a meandering waveguide at multiple coupling points x_m with the external loss rate $\kappa_{m,e}$. The resonator rotates along the CCW direction with an angular speed Ω. The CW and CCW modes of the resonator couple to each other with strength J. The intrinsic decay rate of the resonator is κ_c.

as shown in **Figure 1**. The resonator is rotated and the waveguide is stationary. The separation distance between different coupling points on the waveguide is denoted by $L = x_m - x_n$. We assume the coherence length of photons in the waveguide is larger than the smallest distance $L_{\min}$, and therefore we can ignore the non-Markovian retarded effects [19, 52]. The nonspinning resonator, for example, a whispering-gallery-mode resonator with a resonant frequency ω_c, simultaneously supports both clockwise (CW) and counter-clockwise (CCW) travelling modes. The CW and CCW modes couple to each other through a scatterer or induced by surface roughness [53, 54], which results in an optical mode splitting. When the optical resonator rotates in one direction at an angular velocity Ω, the propagating effects of the CW and CCW modes are different, leading to an opposite Sagnac-Fizeau shift in resonant frequencies, i.e., $\omega_c \to \omega_c + \Delta_F$, with [55].

$$\Delta_F = \pm \frac{nR\Omega\omega_c}{c}\left(1 - \frac{1}{n^2} - \frac{\lambda}{n}\frac{dn}{d\lambda}\right), \tag{1}$$

where n is the refractive index of the dielectric material, R is the radius of the optical resonator, and c (λ) is the velocity (wavelength) of light in vacuum. The dispersion term $\lambda dn/nd\lambda$, denoting the relativistic origin of the Sagnac effect [51, 55], is very small in typical materials compared to the value of $(1-1/n^2)$. In the following we assume the resonator rotates along the CCW direction, hence $\Delta_F > 0$ ($\Delta_F < 0$) represents the case of the driving field coming from the left-hand (right-hand) side. The resonant frequencies of the CW and CCW modes in this situation are $\omega_{cw} = \omega_c + \Delta_F$ and $\omega_{ccw} = \omega_c - \Delta_F$, respectively.

In our consideration, the Hamiltonian of the spinning resonator can be written as ($\hbar = 1$)

$$H_c = (\omega_c + \Delta_F)c_{\rm cw}^{\dagger}c_{\rm cw} + (\omega_c - \Delta_F)c_{\rm ccw}^{\dagger}c_{\rm ccw} + J\left(c_{\rm cw}^{\dagger}c_{\rm ccw} + c_{\rm ccw}^{\dagger}c_{\rm cw}\right). \tag{2}$$

Here $c_{\rm cw}$ and $c_{\rm ccw}$ ($c_{\rm cw}^{\dagger}$ and $c_{\rm ccw}^{\dagger}$) are the annihilation (creation) operators of the CW and CCW modes, respectively. The coupling strength J denotes the interaction between these two modes induced by optical backscattering. The CW (CCW) mode can only be driven by an optical field coming from the left (right) side of the waveguide, own to the directionality of travelling wave modes in the resonator. The driving Hamiltonian is

$$H_d = i\sum_{m=1}^{N}\sqrt{\kappa_{m,e}}c_{m,\rm in}\left(c_{\rm cw}^{\dagger} - c_{\rm cw}\right) + i\sum_{m=1}^{N}\sqrt{\kappa_{m,e}}c'_{m,\rm in}\left(c_{\rm ccw}^{\dagger} - c_{\rm ccw}\right), \tag{3}$$

where $c_{m,\rm in}$ and $c'_{m,\rm in}$ are the input fields coming from the left and right sides at coupling point x_m, respectively. According to Fermi's golden rule [56], $\kappa_{m,e} = 2\pi g_m^2\mathcal{D}(\omega)$ describes the spontaneous emission of the resonator modes into the waveguide at coupling point x_m, with g_m being the resonator-waveguide coupling strength and $\mathcal{D}(\omega)$ being the photon density of states in the waveguide. In the presence of decay channels, the effective non-Hermitian Hamiltonian of the whole system is given by

$$H_1 = H_c + H_d - i\Gamma_c\left(c_{\rm cw}^{\dagger}c_{\rm cw} + c_{\rm ccw}^{\dagger}c_{\rm ccw}\right), \tag{4}$$

with

$$\Gamma_c = \frac{\kappa_c}{2} + \sum_{m=1}^{N}\frac{\kappa_{m,e}}{2}, \tag{5}$$

where Γ_c is the total decay rate of the resonator mode, and κ_c is the intrinsic decay rate of the resonator.

According to the Heisenberg motional equations, the dynamic equations of the CW and CCW modes are yielded by

$$\begin{aligned}\frac{dc_{\rm cw}}{dt} &= -[i(\omega_c + \Delta_F) + \Gamma_c]c_{\rm cw} - iJc_{\rm ccw} + \sum_{m=1}^{N}\sqrt{\kappa_{m,e}}c_{m,\rm in},\\ \frac{dc_{\rm ccw}}{dt} &= -[i(\omega_c - \Delta_F) + \Gamma_c]c_{\rm ccw} - iJc_{\rm cw} + \sum_{m=1}^{N}\sqrt{\kappa_{m,e}}c'_{m,\rm in}.\end{aligned} \tag{6}$$

Note that $k_{\rm cw} = (\omega_c + \Delta_F)/c$ and $k_{\rm ccw} = (\omega_c - \Delta_F)/c$ are approximately regarded as the central mode vector of right-going and left-going photon in the waveguide emitted by the resonator [23], respectively. Different from the case without rotation, the accumulated phase shifts between neighbor coupling points for opposite propagation directions of the photons are distinct. As given in Refs. [17, 57–59], the local input-output relations for the CW and CCW modes at each coupling point x_m are written as

$$\begin{aligned}c_{m,\rm out} &= c_{m,\rm in} - \sqrt{\kappa_{m,e}}c_{\rm cw}, \qquad c_{m+1,\rm in} = c_{m,\rm out}e^{ik_{\rm cw}(x_{m+1}-x_m)},\\ c'_{m,\rm out} &= c'_{m,\rm in} - \sqrt{\kappa_{m,e}}c_{\rm ccw}, \qquad c'_{m,\rm in} = c'_{m+1,\rm out}e^{ik_{\rm ccw}(x_{m+1}-x_m)}.\end{aligned} \tag{7}$$

Substituting **Eq. 7** into **Eq. 6**, we obtain the effective dynamic equations

$$\begin{aligned}\frac{dc_{\rm cw}}{dt} &= -\left[i(\omega_c + \Delta_F) + \Gamma_c + \sum_{m>n=1}^{N}\sqrt{\kappa_{m,e}\kappa_{n,e}}\,e^{ik_{\rm cw}(x_m-x_n)}\right]c_{\rm cw} - iJc_{\rm ccw}\\ &\quad + \sum_{m=1}^{N}\sqrt{\kappa_{m,e}}e^{ik_{\rm cw}(x_m-x_1)}c_{1,\rm in},\\ \frac{dc_{\rm ccw}}{dt} &= -\left[i(\omega_c - \Delta_F) + \Gamma_c + \sum_{m>n=1}^{N}\sqrt{\kappa_{m,e}\kappa_{n,e}}\,e^{ik_{\rm ccw}(x_m-x_n)}\right]c_{\rm ccw} - iJc_{\rm cw}\\ &\quad + \sum_{m=1}^{N}\sqrt{\kappa_{m,e}}e^{ik_{\rm ccw}(x_N-x_m)}c'_{N,\rm in}.\end{aligned} \tag{8}$$

The total input-output relations of this system take the form

$$\begin{aligned}c_{N,\rm out} &= c_{1,\rm in}e^{ik_{\rm cw}(x_N-x_1)} - \sum_{m=1}^{N}\sqrt{\kappa_{m,e}}e^{ik_{\rm cw}(x_N-x_m)}c_{\rm cw},\\ c'_{1,\rm out} &= c'_{N,\rm in}e^{ik_{\rm ccw}(x_N-x_1)} - \sum_{m=1}^{N}\sqrt{\kappa_{m,e}}e^{ik_{\rm ccw}(x_m-x_1)}c_{\rm ccw}.\end{aligned} \tag{9}$$

Eq. 8 exhibits a self-coupling in the CW or CCW mode, which arises from the self interference effects of reemitted photons between different connection points. Moreover, the Sagnac effect and the self-interference effects may significantly affect the optical properties of the system. We note that only when the resonator is nonspinning, the system is reciprocal. Based on these derivations, we will investigate the photon emission and transport properties in this system.

2.2 Phase Controlled Chiral Emission

In the giant-atom waveguide-QED systems, the multiple coupling points result in a frequency-dependent decay rate and Lamb shift for a giant atom [23, 60]. Similarly, the interference effects induced by multiple coupling points in our system also give a modification of the frequency shift Δ_j and decay rate Γ_j for the CW and CCW mode. According to **Eq. 8**, we have

$$\begin{aligned}\Delta_j &= \sum_{m>n=1}^{N}\sqrt{\kappa_{m,e}\kappa_{n,e}}\sin\left(\phi_{mn}^{j}\right),\\ \Gamma_j &= \Gamma_c + \sum_{m>n=1}^{N}\sqrt{\kappa_{m,e}\kappa_{n,e}}\cos\left(\phi_{mn}^{j}\right).\end{aligned} \tag{10}$$

where $\phi_{mn}^{j} = k_j(x_m - x_n)$ with j = cw, ccw.

Here we consider the maximally symmetric case, in which decay rates of the resonator modes into the waveguide are the same at each coupling point with $\kappa_{m,e} = \kappa_e$ and the distance between neighboring coupling points is identical with $x_{m+1} - x_m = d$. Then we can set $x_m - x_n = (m-n)d$ and $\theta_j = k_j d$. Similar to the Lamb shift and decay rate in atomic physics, **Eq. 10** becomes

$$\begin{aligned}\Delta_j &= \frac{\kappa_e}{2}\left[\frac{N\sin\left(\theta_j\right) - \sin\left(N\theta_j\right)}{1 - \cos\left(\theta_j\right)}\right],\\ \Gamma_j &= \frac{\kappa_c}{2} + \frac{\kappa_e}{2}\left[\frac{1 - \cos\left(N\theta_j\right)}{1 - \cos\left(\theta_j\right)}\right].\end{aligned} \tag{11}$$

We begin to discuss the effects of the rotation speed and number of coupling points on the emission properties under the condition of $\kappa_c = 0$. When the resonator is nonspinning with $\Omega = 0$, the CW

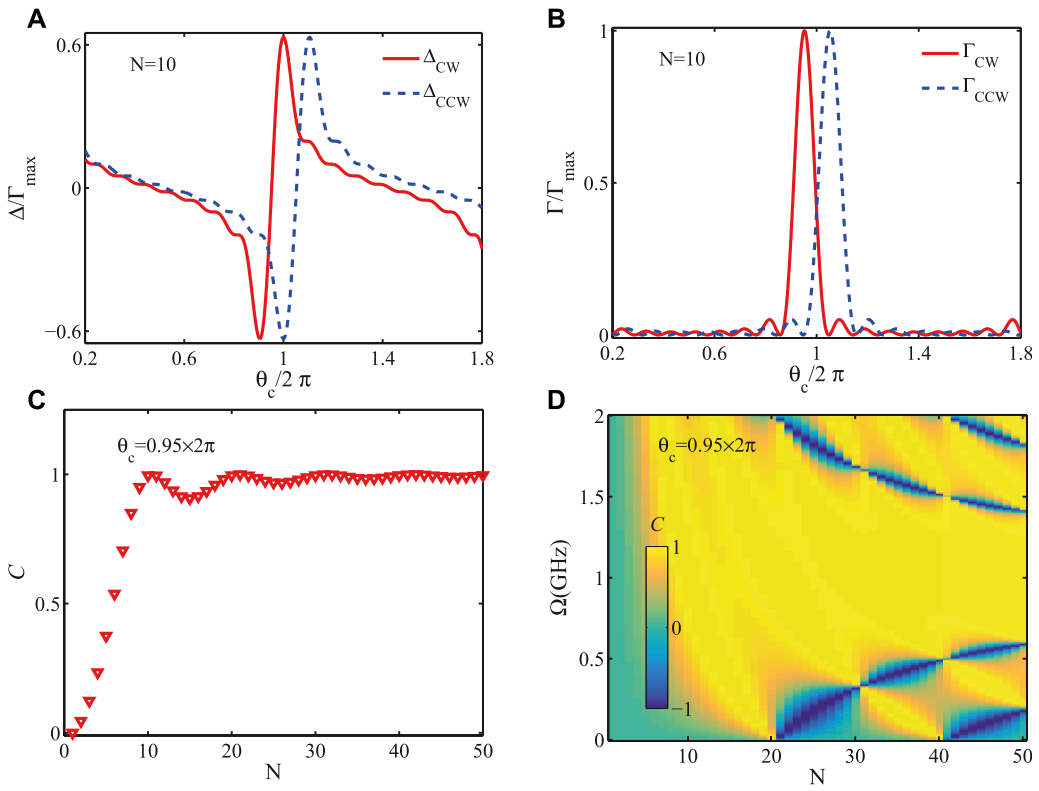

FIGURE 2 | (Color online) The frequency shifts Δ_j **(A)** and the decay rates Γ_j **(B)** for the CW and CCW modes versus phase $\theta_c = \omega_c d/c$ for $N = 10$ and $\Omega = 0.97$ GHz. The maximum decay rate Γ_{cw} is used for normalization. **(C)** The chiral factor $\mathcal{C}$ changes with number of coupling points N. **(D)** The chiral factor $\mathcal{C}$ versus N and rotation speed Ω are plotted. Other parameters are set as: λ = 1,550 nm, R = 4.73 mm, n = 1.4, and $\kappa_c = 0$.

and CCW modes are degenerate with the Fizeau drag $\Delta_F = 0$ and $\omega_{ccw} = \omega_{cw} = \omega_c$. As increasing the rotation speed Ω, the Sagnac-Fizeau shift described by **Eq. 1** linearly increases, as given in **Supplementary Material**. In our calculations, we choose the related parameters as follows: λ = 1,550 nm, R = 4.73 mm, and n = 1.4. For $\Omega = 0.97$ GHz, we have $\Delta_F/\omega_c = \pm 0.05$ and $(R\Omega)/c \approx 0.015$. For the spinning resonator with a single coupling point ($N = 1$), **Eq. 11** gives the results of $\Delta_{cw} = \Delta_{ccw} = 0$ and $\Gamma_{cw} = \Gamma_{ccw} = (\kappa_c + \kappa_e)/2$. When increasing the number of coupling points, the frequency shifts and decay rates for the CW and CCW modes have an opposite shift due to the rotation.

In **Figures 2A,B**, frequency shifts Δ_j and decay rates Γ_j are plotted as a function of the phase $\theta_c = \omega_c d/c$ with $N = 10$ and $\Omega = 0.97$ GHz. The frequency shifts Δ_{cw} and Δ_{ccw} take negative and positive values with the maximum at about $0.6\Gamma_{max}$. Given that Δ_{cw} (Δ_{ccw}) is zero, the decay rate Γ_{cw} (Γ_{ccw}) reaches its highest magnitude at $\theta_c = 0.95 \times 2\pi$ ($\theta_c = 1.05 \times 2\pi$). For $\theta_c = 0.95 \times 2\pi$, the accumulated phase of photons propagating along the CCW direction leads to $\Gamma_{ccw} = 0$, which arises from the destructive interference effects among the coupling points. In this case, the CCW mode of the resonator is decoupled from the waveguide. Moreover, there are a lot of additional lower and local maximum values in the decay rates. The phase θ_c of the local minima between these maxima scales with $(1/N + \Delta_F/\omega_c)$. Note that the rotation speed and number of coupling points make a big difference in the values of Γ_{cw} and Γ_{ccw}. Narrower resonances can be found in the decay rates when we consider more coupling points.

In order to study the emission properties more clearly, for a special frequency we define the chirality parameter $\mathcal{C}$ as

$$\mathcal{C} = \frac{\Gamma_{cw} - \Gamma_{ccw}}{\Gamma_{cw} + \Gamma_{ccw}}, \tag{12}$$

where $\mathcal{C} = 1$ ($\mathcal{C} = -1$) implies a truly unidirectional excitation of the right-going (left-going) photon, and $\mathcal{C} = 0$ denotes the photon coupling into the waveguide without preference in both propagating directions. **Figure 2C** depicts the chiral factor $\mathcal{C}$ changing with number of coupling points N. When $N = 1$, the chiral factor is $\mathcal{C} = 0$. For $\theta_c = 0.95 \times 2\pi$, as increasing number of coupling points N, the chirality factor $\mathcal{C}$ first goes up and then oscillates slowly with a relative larger value around 1. Note that $\mathcal{C} = 1$ is obtained for $N = 10$, corresponding to $\Gamma_{cw} = 50\kappa_e$ and $\Gamma_{ccw} = 0$. The essence of the chirality is that accumulated phases for photons propagating in CW and CCW directions are different. By tuning the phase shift θ_c, for example, $\theta_c = 1.05 \times 2\pi$, the photon emission direction is

totally switched. **Figure 2D** shows the chiral factor $\mathcal{C}$ as functions of number of coupling points N and rotation speed Ω for $\theta_c = 0.95 \times 2\pi$. By optimizing the rotation speed and number of coupling points, the chiral factor $\mathcal{C}$ can approach 1, and the chiral direction can be freely switched. Moreover, the directional emission will be realized in a large parameter regime.

2.3 Nonreciprocal Photon Transmission

Now we study how the rotation velocity and number of coupling points affect the optical response of the spinning resonator. We consider the resonator is excited by an external input signal in the CW direction with frequency ω_l and amplitude ε. In this case, the input signal from the left side is given by $c_{1,\text{in}} + \varepsilon e^{-i\omega_l t}$, with $c_{1,\text{in}}$ being the vacuum input signal, while the input signal from the right side only contains the vacuum input field $c'_{N,\text{in}}$. In the rotating frame at the driving frequency ω_l, the steady-state solutions of **Eq. 8** can be written as

$$\langle c_{\text{cw}} \rangle = \frac{[i(\Delta_c - \Delta_F + \Delta_{\text{ccw}}) + \Gamma_{\text{ccw}}] \sum_{m=1}^{N} \sqrt{\kappa_{m,e}} e^{ik_{\text{cw}}(x_m - x_1)} \varepsilon}{[i(\Delta_c - \Delta_F + \Delta_{\text{ccw}}) + \Gamma_{\text{ccw}}][i(\Delta_c + \Delta_F + \Delta_{\text{cw}}) + \Gamma_{\text{cw}}] + J^2}. \tag{13}$$

Here $\Delta_c = \omega_c - \omega_l$ is the detuning between the resonator without rotation and the driving field. The transmission rate of the input signal is given by

$$T_L = \left| \frac{\langle c_{N,\text{out}} \rangle}{\varepsilon} \right|^2 = \left| 1 - \frac{[i(\Delta_c - \Delta_F + \Delta_{\text{ccw}}) + \Gamma_{\text{ccw}}] \sum_{m,\ n=1}^{N} \sqrt{\kappa_{m,e}\kappa_{n,e}}\, e^{ik_{\text{cw}}(x_m - x_n)}}{[i(\Delta_c - \Delta_F + \Delta_{\text{ccw}}) + \Gamma_{\text{ccw}}][i(\Delta_c + \Delta_F + \Delta_{\text{cw}}) + \Gamma_{\text{cw}}] + J^2} \right|^2. \tag{14}$$

Similarly, we also consider the case of an external input signal coming from the right side of the waveguide with $\varepsilon' e^{-i\omega_l t}$. By solving the steady-state solutions of **Eq. 8**, we obtain

$$\langle c_{\text{ccw}} \rangle = \frac{[i(\Delta_c + \Delta_F + \Delta_{\text{cw}}) + \Gamma_{\text{cw}}] \sum_{m=1}^{N} \sqrt{\kappa_{m,e}} e^{ik_{\text{ccw}}(x_N - x_m)} \varepsilon'}{[i(\Delta_c - \Delta_F + \Delta_{\text{ccw}}) + \Gamma_{\text{ccw}}][i(\Delta_c + \Delta_F + \Delta_{\text{cw}}) + \Gamma_{\text{cw}}] + J^2}. \tag{15}$$

The transmission rate of the input signal is written as

$$T_R = \left| \frac{\langle c'_{1,\text{out}} \rangle}{\varepsilon'} \right|^2 = \left| 1 - \frac{[i(\Delta_c + \Delta_F + \Delta_{\text{cw}}) + \Gamma_{\text{cw}}] \sum_{m,\ n=1}^{N} \sqrt{\kappa_{m,e}\kappa_{n,e}}\, e^{ik_{\text{ccw}}(x_m - x_n)}}{[i(\Delta_c - \Delta_F + \Delta_{\text{ccw}}) + \Gamma_{\text{ccw}}][i(\Delta_c + \Delta_F + \Delta_{\text{cw}}) + \Gamma_{\text{cw}}] + J^2} \right|^2. \tag{16}$$

A nonreciprocal photon transmission with $T_R \neq T_L$ can be observed when the resonator is spinning. This fact is due to the different numerators in **Eqs 13**, **15**. For the maximally symmetric case, we have

$$\Gamma'_j = \sum_{m,\ n=1}^{N} \sqrt{\kappa_{m,e}\kappa_{n,e}} e^{ik_j(x_m - x_n)} = \kappa_e \left[\frac{1 - \cos(N\theta_j)}{1 - \cos(\theta_j)} \right]. \tag{17}$$

For $J = 0$, the incident photon will be transmitted and absorbed with reflection being zero. In this scenario, the transmission curve T_L represents a Lorentzian line shape centered at $\Delta_c = -(\Delta_F + \Delta_{\text{cw}})$ with a linewidth Γ_{cw}. For $N = 1$, we obtain $\Delta_c = -\Delta_F$ and $\Gamma_{\text{cw}} = (\kappa_c + \kappa_e)/2$. The transmission dip is around 0. For multiple coupling points, as discussed above, Δ_{cw} and Γ_{cw} vary periodically with phase θ_c. The transmission rate T_L versus the detuning Δ_c and the phase θ_c are plotted in **Figure 3A**. It shows that θ_c will dramatically modify the transmission window. As we increase θ_c, the position of the transmission dip has a red-shift. When the phase θ_{cw} is $2\pi/N$, the transmission dip disappears totally with $T = 1$, which means the resonator cannot be excited by the external field and corresponds to the optical dark state. This phenomenon arises from the destructive interferences in the multiple coupling points, which can be explained by **Eq. 17**. Moreover, the mode splitting is observed in some parameter range in **Figure 3B** when $J = 5\kappa_e$. The asymmetry of the two dips results from different decay rates and frequency shifts of these two modes.

In **Figures 3C,D**, we plot the transmission rates T_L and T_R when the incident photon coming from the left side and right sides versus the detuning Δ_c for $\theta = 0.95 \times 2\pi$. It shows that T_L can be larger or smaller than T_R for $N = 5$. In other words, the nonreciprocal transmission is clearly observed due to the rotation. The interference effects between coupling points enable the transmission dips asymmetric with different linewidths. For $N = 10$, the decay rate of the CCW mode is very small, which leads to the complete photon transmission with $T_R = 1$. Moreover, a sharp dip appears in the transmission spectra T_L for $J = 5\kappa_e$. Note that the phase θ_c can also be used to adjust the nonreciprocal transmission behavior.

3 TWO SPINNING RESONATORS INTERACTING WITH MULTIPLE POINTS

3.1 Hamiltonian and Dynamic Equations

The single-photon transport properties in a one-dimensional waveguide interacted with two giant atoms for three distinct topologies have been discussed in Ref. [61]. To study potential applications of the spinning resonator with multiple coupling points in large-scale quantum chiral networks, we now consider two separate spinning resonators evanescently coupled to a meandering waveguide at several different connection points. As shown in **Figure 4**, the optical resonator a (b) simultaneously supports both clockwise and counter-clockwise travelling optical modes. The creation operators of the CW and CCW modes are denoted by $a^\dagger_{\text{cw}}$ and $a^\dagger_{\text{ccw}}$ ($b^\dagger_{\text{cw}}$ and $b^\dagger_{\text{ccw}}$), respectively. The optical resonator a (b), with stationary resonant frequency ω_a (ω_b) and intrinsic decay rate κ_a (κ_b), rotates along the CCW direction by an angular velocity Ω_a (Ω_b). Owing to the rotation, the resonant frequencies of the CW and CCW modes in the resonator become $\omega_{i,\text{cw}} = \omega_i + \Delta_{F,i}$ and $\omega_{i,\text{ccw}} = \omega_i - \Delta_{F,i}$ with the subscript $i = a, b$, where $\Delta_{F,i}$ is given by **Eq. 1**. The resonator a (b) is coupled to the bent waveguide at connection points x^a_1 and x^a_2 (x^b_1 and x^b_2). The phase factor ϕ_i is calculated as $k(x^i_1 - x^i_2)$when an optical signal travelling between them, and the phase factor when photons travelling from resonator a to resonator b is $\phi_L = k(x^b_1 - x^a_2)$. Here we note that there is no direct coupling between cavity a and cavity b due to the absence of the modal overlap.

The Hamiltonian of these two spinning resonators are given by

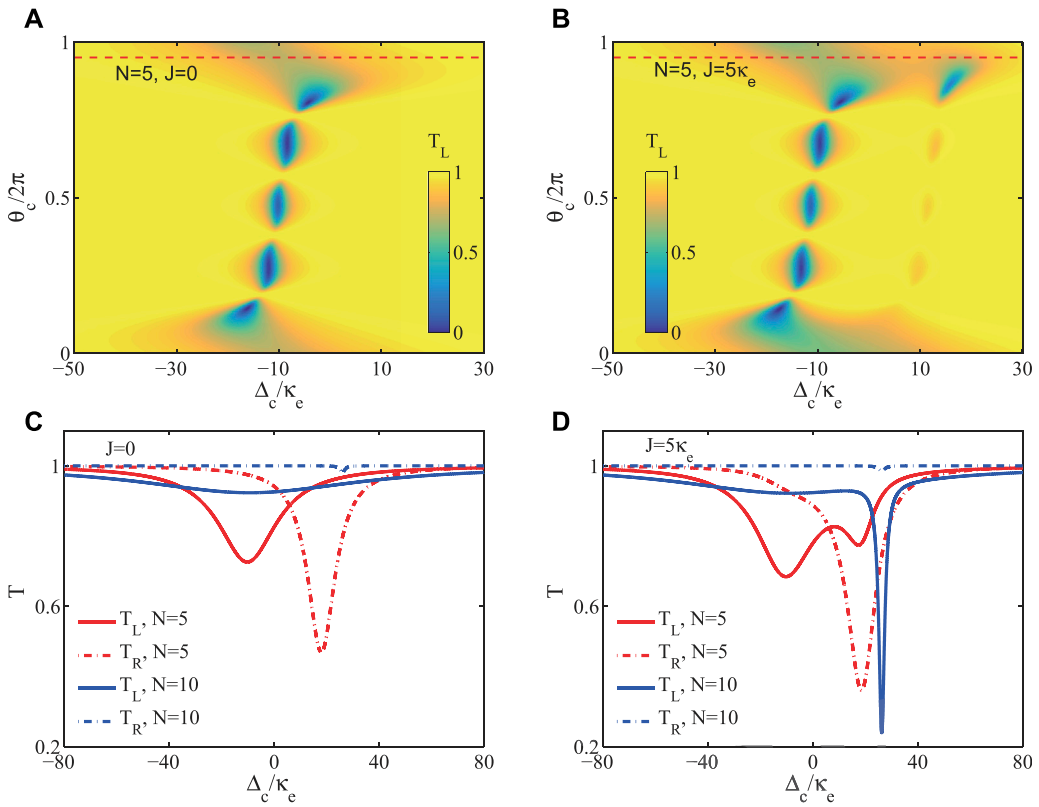

FIGURE 3 | (Color online) Transmission rate T_R versus detuning Δ_c/κ and phase $\theta_c/2\pi$ for different coupling stengths: **(A)** $J = 0$, and **(B)** $J = 5\kappa_e$. Profiles of T_R and T_L versus Δ_c/κ with $\theta_c = 0.95 \times 2\pi$: **(C)** $J = 0$ and **(D)** $J = 5\kappa_e$. Other parameters are set as: $\kappa_e = 5 \times 10^{-3}\omega_c$, $\Omega = 0.97$ GHz, and $\kappa_c = 2\kappa_e$.

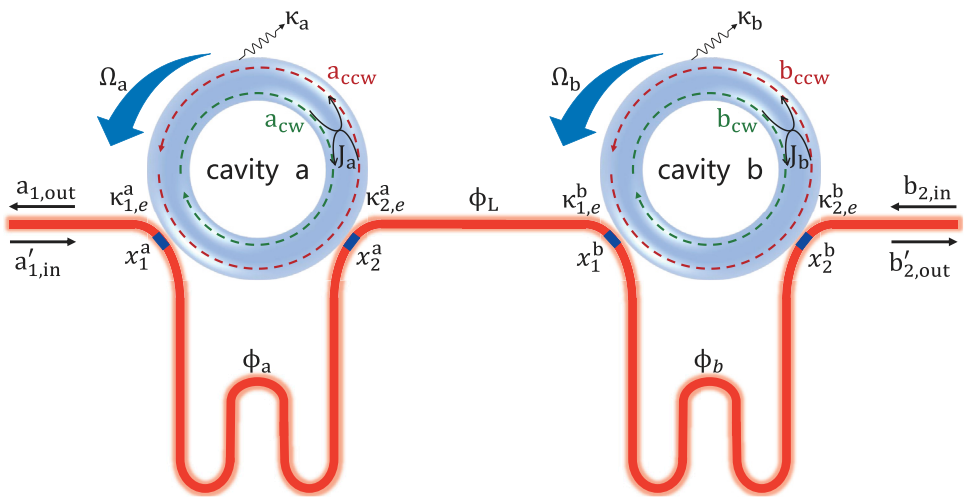

FIGURE 4 | (Color online) Schematic of two separate spinning resonators coupled to a meandering waveguide at several coupling points x_i^a and x_i^b with $i = 1, 2$. The resonator a (b) with the intrinsic decay rate κ_a (κ_b) rotates along the CCW direction at an angular speed Ω_a (Ω_b). The CW and CCW modes of the resonator a (b) couple to each other with strength J_a (J_b). The external loss rates at coupling points x_i^a and x_i^b are $\kappa_{i,e}^a$ and $\kappa_{i,e}^b$, respectively. For the photon in the waveguide, the distance between neighboring coupling points results in different propagation phases denoting by ϕ_a, ϕ_L, and ϕ_b. Note that $\{a_{1,\text{in}}', b_{2,\text{in}}\}$ and $\{b_{2,\text{out}}', a_{1,\text{out}}\}$ are the input and output operators of optical fields towards and away the resonators.

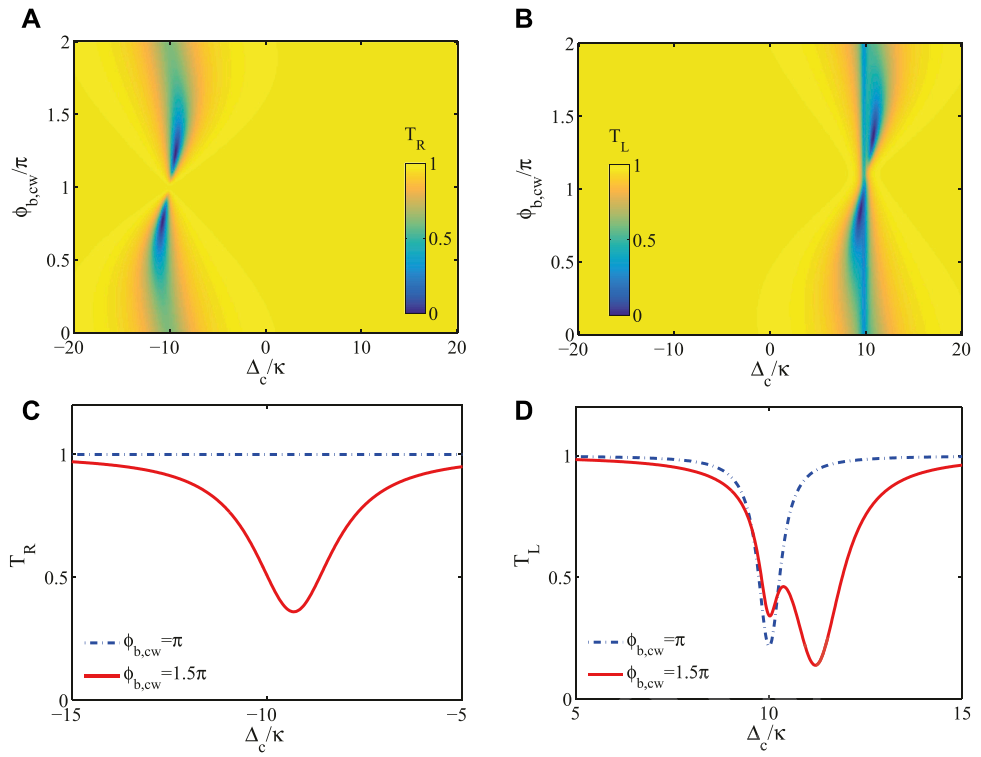

FIGURE 5 | (Color online) Transmission rates T_R **(A)** and T_L **(B)** versus the detuning Δ_c/κ and the phase $\phi_{b,cw}/\pi$. The corresponding transmission rates as a function of detuning Δ_c/κ for different phases $\phi_{b,cw}/\pi$ are plotted in **(C,D)**. The parameters are set as: $\kappa = 5\times10^{-3}\omega_c$, $\Omega = 0.97$ GHz, $\kappa^i_{j,e} = \kappa$, $\kappa_i = 0.5\kappa$, and $\phi_{a,cw} = \phi_{L,cw} = \pi$ with $i = a, b$ and $j = 1, 2$.

$$H_c' = \sum_{j=cw,ccw}\left(\omega_{a,j}a_j^\dagger a_j + \omega_{b,j}b_j^\dagger b_j\right) + J_a\left(a_{cw}^\dagger a_{ccw} + a_{ccw}^\dagger a_{cw}\right) + J_b\left(b_{cw}^\dagger b_{ccw} + b_{ccw}^\dagger b_{cw}\right). \tag{18}$$

Here J_a (J_b) is the coupling strength between the CW and CCW modes of the resonator a (b). The CCW (CW) modes in the resonators can only be driven by an optical field coming from the left (right) side of the waveguide. The amplitudes of the input fields at different coupling points are denoted by $a_{m,in}$, $b_{m,in}$, $a'_{m,in}$, and $b'_{m,in}$ with $m = 1, 2$. The driving fields give the Hamiltonian

$$H_d' = i\sum_{m=1}^{2}\sqrt{\kappa^a_{m,e}}a_{m,in}\left(a_{cw}^\dagger - a_{cw}\right) + i\sum_{m=1}^{2}\sqrt{\kappa^a_{m,e}}a'_{m,in}\left(a_{ccw}^\dagger - a_{ccw}\right) + i\sum_{m=1}^{2}\sqrt{\kappa^b_{m,e}}b_{m,in}\left(b_{cw}^\dagger - b_{cw}\right) + i\sum_{m=1}^{2}\sqrt{\kappa^b_{m,e}}b'_{m,in}\left(b_{ccw}^\dagger - b_{ccw}\right). \tag{19}$$

The non-Hermitian Hamiltonian of the whole system can be given by

$$H_2 = H_c' + H_d' - i\Gamma_a\left(a_{cw}^\dagger a_{cw} + a_{ccw}^\dagger a_{ccw}\right) - i\Gamma_b\left(b_{cw}^\dagger b_{cw} + b_{ccw}^\dagger b_{ccw}\right), \tag{20}$$

where $\Gamma_i = (\kappa_i + \kappa^i_{1,e} + \kappa^i_{2,e})/2$ and $i = a, b$. Note that κ_a (κ_b) is the intrinsic optical loss of the resonator a (b), $\kappa^i_{1,e}$ and $\kappa^i_{2,e}$ are the waveguide-resonator coupling rates at coupling points x^i_1 and x^i_2, respectively.

The effective dynamic evolution equations of the cavity modes can be written as

$$\begin{aligned}
\frac{da_{cw}}{dt} &= -\left[i(\omega_a + \Delta_{F,a}) + \Gamma_a + \sqrt{\kappa^a_{1,e}\kappa^a_{2,e}}\,e^{i\phi_{a,cw}}\right]a_{cw} - iJ_a a_{ccw} - F_{cw}b_{cw} + \left[\sqrt{\kappa^a_{1,e}}\,e^{i\left(\phi_{a,cw}+\phi_{L,cw}+\phi_{b,cw}\right)} + \sqrt{\kappa^a_{2,e}}\,e^{i\left(\phi_{L,cw}+\phi_{b,cw}\right)}\right]b_{2,in},\\
\frac{da_{ccw}}{dt} &= -\left[i(\omega_a - \Delta_{F,a}) + \Gamma_a + \sqrt{\kappa^a_{1,e}\kappa^a_{2,e}}\,e^{i\phi_{a,ccw}}\right]a_{ccw} - iJ_a a_{cw} + \left(\sqrt{\kappa^a_{1,e}} + \sqrt{\kappa^a_{2,e}}\,e^{i\phi_{a,ccw}}\right)a'_{1,in},\\
\frac{db_{cw}}{dt} &= -\left[i(\omega_b + \Delta_{F,b}) + \Gamma_b + \sqrt{\kappa^b_{1,e}\kappa^b_{2,e}}\,e^{i\phi_{b,cw}}\right]b_{cw} - iJ_b b_{ccw} + \left(\sqrt{\kappa^b_{1,e}}\,e^{i\phi_{b,cw}} + \sqrt{\kappa^b_{2,e}}\right)b_{2,in},\\
\frac{db_{ccw}}{dt} &= -\left[i(\omega_b - \Delta_{F,b}) + \Gamma_b + \sqrt{\kappa^b_{1,e}\kappa^b_{2,e}}\,e^{i\phi_{b,ccw}}\right]b_{ccw} - iJ_b b_{cw} - F_{ccw}a_{ccw} + \left[\sqrt{\kappa^b_{1,e}}\,e^{i\left(\phi_{a,ccw}+\phi_{L,ccw}\right)} + \sqrt{\kappa^b_{2,e}}\,e^{i\left(\phi_{a,ccw}+\phi_{L,ccw}+\phi_{b,ccw}\right)}\right]a'_{1,in},
\end{aligned} \tag{21}$$

where

$$F_j = \sqrt{\kappa^a_{1,e}\kappa^b_{1,e}}e^{i\left(\phi_{a,j}+\phi_{L,j}\right)} + \sqrt{\kappa^a_{1,e}\kappa^b_{2,e}}e^{i\left(\phi_{a,j}+\phi_{L,j}+\phi_{b,j}\right)} + \sqrt{\kappa^a_{2,e}\kappa^b_{1,e}}e^{i\phi_{L,j}} + \sqrt{\kappa^a_{2,e}\kappa^b_{2,e}}e^{i\left(\phi_{L,j}+\phi_{b,j}\right)}. \tag{22}$$

Note that F_{cw} (F_{ccw}) denotes the effective unidirectional coupling strength between the CW (CCW) modes of these two resonators. The total input-output relations of this system take the form

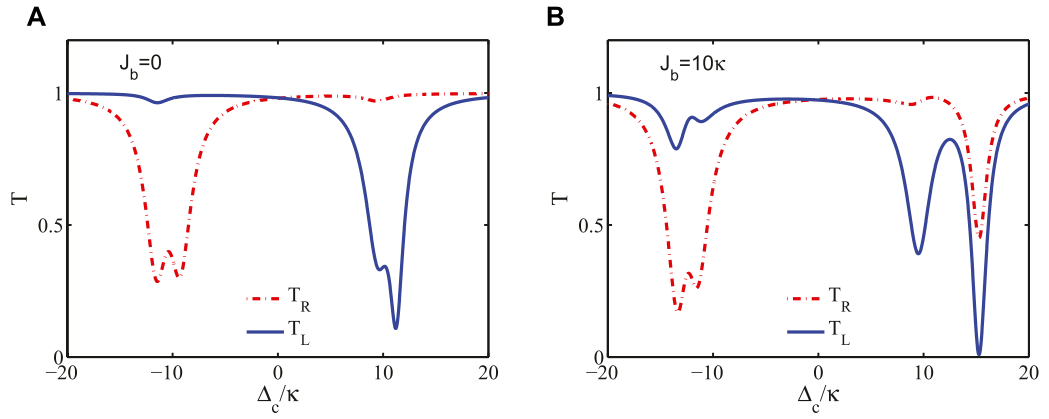

FIGURE 6 | (Color online) The transmission rates T_R and T_L versus the detuning Δ_c/κ for **(A)** $J_b = 0$ and **(B)** $J_b = 10\kappa$. The parameters are set as: $\kappa = 5 \times 10^{-3}\omega_c$, $\Omega = 0.97$ GHz, $\kappa_{j,e}^{i} = \kappa$, $\kappa_i = 0.5\kappa$, $J_a = 2\kappa$, $\phi_{a,\mathrm{cw}} = 0.5\pi$, $\phi_{L,\mathrm{cw}} = \pi$, and $\phi_{b,\mathrm{cw}} = 1.5\pi$ with $i = a, b$ and $j = 1, 2$.

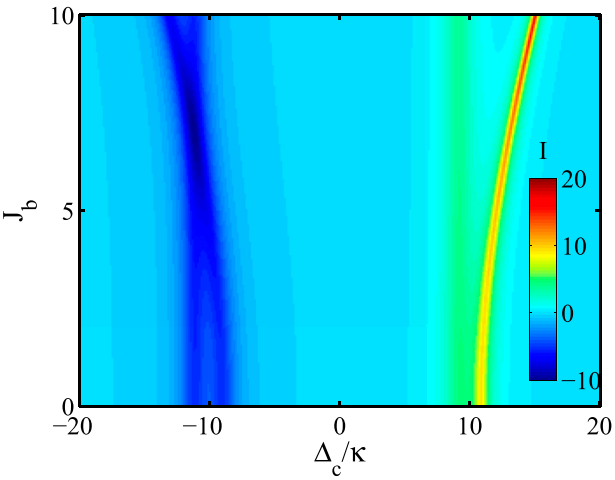

FIGURE 7 | (Color online) The isolation ratio $\mathcal{I}$ as functions of the detuning Δ_c/κ and the coupling strength J_b. The parameters are set as: $\kappa = 5 \times 10^{-3}\omega_c$, $\Omega = 0.97$ GHz, $\kappa_{j,e}^{i} = \kappa$, $\kappa_i = 0.5\kappa$, $J_a = 2\kappa$, $\phi_{a,\mathrm{cw}} = 0.5\pi$, $\phi_{L,\mathrm{cw}} = \pi$, and $\phi_{b,\mathrm{cw}} = 1.5\pi$ with $i = a, b$ and $j = 1, 2$.

$$
\begin{aligned}
a_{1,\mathrm{out}} &= b_{2,\mathrm{in}} e^{i\left(\phi_{a,\mathrm{cw}}+\phi_{L,\mathrm{cw}}+\phi_{b,\mathrm{cw}}\right)} - \left(\sqrt{\kappa_{1,e}^{a}} + \sqrt{\kappa_{2,e}^{a}}\, e^{i\phi_{a,\mathrm{cw}}}\right) a_{\mathrm{cw}} \\
&\quad - \left[\sqrt{\kappa_{1,e}^{b}}\, e^{i\left(\phi_{a,\mathrm{cw}}+\phi_{L,\mathrm{cw}}\right)} + \sqrt{\kappa_{2,e}^{b}}\, e^{i\left(\phi_{a,\mathrm{cw}}+\phi_{L,\mathrm{cw}}+\phi_{b,\mathrm{cw}}\right)}\right] b_{\mathrm{cw}}, \\
b'_{2,\mathrm{out}} &= a'_{1,\mathrm{in}} e^{i\left(\phi_{a,\mathrm{ccw}}+\phi_{L,\mathrm{ccw}}+\phi_{b,\mathrm{ccw}}\right)} - \left(\sqrt{\kappa_{2,e}^{b}} + \sqrt{\kappa_{1,e}^{b}}\, e^{i\phi_{b,\mathrm{ccw}}}\right) b_{\mathrm{ccw}} \\
&\quad - \left(\sqrt{\kappa_{2,e}^{a}}\, e^{i\left(\phi_{L,\mathrm{ccw}}+\phi_{b,\mathrm{ccw}}\right)} + \sqrt{\kappa_{1,e}^{a}}\, e^{i\left(\phi_{a,\mathrm{ccw}}+\phi_{L,\mathrm{ccw}}+\phi_{b,\mathrm{ccw}}\right)}\right) a_{\mathrm{ccw}}.
\end{aligned}
\tag{23}
$$

By using **Eqs 21**, **23**, we can investigate the photon transport properties of this system in the steady state.

3.2 Nonreciprocal Photon Transmission

In the following, we consider the input signal only comes from one side of the waveguide. Supposed that an external input signal $b_{2,\mathrm{in}}$ is injected from the right side of the waveguide with $\varepsilon e^{-i\omega_l t}$, where ε and ω_l are the amplitude and frequency of the driving field, respectively. In the rotating frame at the driving frequency ω_b the steady-state solutions of the CW resonator modes in **Eq. 21** are solved as

$$
\begin{aligned}
\langle a_{\mathrm{cw}} \rangle &= \frac{U_{\mathrm{ccw}}\left(V_{\mathrm{cw}}V_{\mathrm{ccw}} + J_b^2\right)A_{\mathrm{cw}} - U_{\mathrm{ccw}}V_{\mathrm{ccw}}F_{\mathrm{cw}}B_{\mathrm{cw}}}{\left(U_{\mathrm{cw}}U_{\mathrm{ccw}} + J_a^2\right)\left(V_{\mathrm{cw}}V_{\mathrm{ccw}} + J_b^2\right) + J_aJ_bF_{\mathrm{cw}}F_{\mathrm{ccw}}}\varepsilon, \\
\langle b_{\mathrm{cw}} \rangle &= \frac{V_{\mathrm{ccw}}\left(U_{\mathrm{cw}}U_{\mathrm{ccw}} + J_a^2\right)B_{\mathrm{cw}} + J_aJ_bF_{\mathrm{ccw}}A_{\mathrm{cw}}}{\left(U_{\mathrm{cw}}U_{\mathrm{ccw}} + J_a^2\right)\left(V_{\mathrm{cw}}V_{\mathrm{ccw}} + J_b^2\right) + J_aJ_bF_{\mathrm{cw}}F_{\mathrm{ccw}}}\varepsilon,
\end{aligned}
\tag{24}
$$

where

$$
\begin{aligned}
U_{\mathrm{cw}} &= i\left(\Delta_a + \Delta_{F,a}\right) + \Gamma_a + \sqrt{\kappa_{1,e}^{a}\kappa_{2,e}^{a}}\, e^{i\phi_{a,\mathrm{cw}}}, \\
U_{\mathrm{ccw}} &= i\left(\Delta_a - \Delta_{F,a}\right) + \Gamma_a + \sqrt{\kappa_{1,e}^{a}\kappa_{2,e}^{a}}\, e^{i\phi_{a,\mathrm{ccw}}}, \\
V_{\mathrm{cw}} &= i\left(\Delta_b + \Delta_{F,b}\right) + \Gamma_b + \sqrt{\kappa_{1,e}^{b}\kappa_{2,e}^{b}}\, e^{i\phi_{b,\mathrm{cw}}}, \\
V_{\mathrm{ccw}} &= i\left(\Delta_b - \Delta_{F,b}\right) + \Gamma_b + \sqrt{\kappa_{1,e}^{b}\kappa_{2,e}^{b}}\, e^{i\phi_{b,\mathrm{ccw}}}, \\
A_{\mathrm{cw}} &= \sqrt{\kappa_{1,e}^{a}}\, e^{i\left(\phi_{a,\mathrm{cw}}+\phi_{L,\mathrm{cw}}+\phi_{b,\mathrm{cw}}\right)} + \sqrt{\kappa_{2,e}^{a}}\, e^{i\left(\phi_{L,\mathrm{cw}}+\phi_{b,\mathrm{cw}}\right)}, \\
A_{\mathrm{ccw}} &= \sqrt{\kappa_{1,e}^{a}} + \sqrt{\kappa_{2,e}^{a}}\, e^{i\phi_{a,\mathrm{ccw}}}, \\
B_{\mathrm{cw}} &= \sqrt{\kappa_{1,e}^{b}}\, e^{i\phi_{b,\mathrm{cw}}} + \sqrt{\kappa_{2,e}^{b}}, \\
B_{\mathrm{ccw}} &= \sqrt{\kappa_{1,e}^{b}}\, e^{i\left(\phi_{a,\mathrm{ccw}}+\phi_{L,\mathrm{ccw}}\right)} + \sqrt{\kappa_{2,e}^{b}}\, e^{i\left(\phi_{a,\mathrm{ccw}}+\phi_{L,\mathrm{ccw}}+\phi_{b,\mathrm{ccw}}\right)}.
\end{aligned}
\tag{25}
$$

Here, $\Delta_a = \omega_a - \omega_l$ ($\Delta_b = \omega_b - \omega_l$) is the detuning between the resonator a (b) without rotation and the driving field. According to **Eq. 23**, the transmission rate of the output port $a_{1,\mathrm{out}}$ for the input signal $b_{2,\mathrm{in}}$ can be defined as $T_R = |\langle a_{1,\mathrm{out}}\rangle/\varepsilon|^2$.

Similarly, when an external input signal is injected from the left side of the waveguide with $\varepsilon' e^{-i\omega_l t}$, the steady-state solutions of the CCW resonator modes in **Eq. 21** are also solved as

$$
\begin{aligned}
\langle a_{\mathrm{ccw}} \rangle &= \frac{U_{\mathrm{cw}}\left(V_{\mathrm{cw}}V_{\mathrm{ccw}} + J_b^2\right)A_{\mathrm{ccw}} + J_aJ_bF_{\mathrm{cw}}B_{\mathrm{ccw}}}{\left(U_{\mathrm{cw}}U_{\mathrm{ccw}} + J_a^2\right)\left(V_{\mathrm{cw}}V_{\mathrm{ccw}} + J_b^2\right) + J_aJ_bF_{\mathrm{cw}}F_{\mathrm{ccw}}}\varepsilon', \\
\langle b_{\mathrm{ccw}} \rangle &= \frac{V_{\mathrm{cw}}\left(U_{\mathrm{cw}}U_{\mathrm{ccw}} + J_a^2\right)B_{\mathrm{ccw}} - U_{\mathrm{cw}}V_{\mathrm{cw}}F_{\mathrm{ccw}}A_{\mathrm{ccw}}}{\left(U_{\mathrm{cw}}U_{\mathrm{ccw}} + J_a^2\right)\left(V_{\mathrm{cw}}V_{\mathrm{ccw}} + J_b^2\right) + J_aJ_bF_{\mathrm{cw}}F_{\mathrm{ccw}}}\varepsilon',
\end{aligned}
\tag{26}
$$

Once again, the transmission rate of the ouput port $b'_{2,\text{out}}$ is given by $T_L = |\langle b'_{2,\text{out}}\rangle/\varepsilon'|^2$.

In the following, we choose the related parameters as follows: $\omega_a = \omega_b = \omega_c$, $\Omega_a = \Omega_b = 0.97$ GHz, $\kappa^a_{m,e} = \kappa^b_{m,e} = \kappa$, $\kappa_a = \kappa_b = 0.5\kappa$, $\kappa = 5 \times 10^{-3}\omega_c$ and $\phi_{L,\text{cw}} = \pi$. Thus, $\Delta_a = \Delta_b = \Delta_c$ and $\Delta_{F,a} = \Delta_{F,b}$. We first consider the CW and CCW modes decoupling, i.e., $J_a = J_b = 0$. In **Figures 5A,B**, we plot the transmission rates T_R and T_L versus the detuning Δ_c/κ and the phase $\phi_{b,\text{cw}}/\pi$ for $\phi_{a,\text{cw}} = \pi$. According to **Eqs 23**, **24**, the transmission rate T_R represents a Lorentzian line shape centered at $\Delta_c = -\Delta_F - \kappa \sin(\phi_{b,\text{cw}})$ with a linewidth $\Gamma_b + \kappa\cos(\phi_{b,\text{cw}})$. However, the behavior of transmission rate T_L is different. A mode splitting may appear around $\Delta_c = \Delta_F$, which implies indirect coherent coupling between the CCW modes of these two resonators is achieved. The reason behind this phenomenon is that the phase $\phi_{a,\text{ccw}}$ is not equal to π own to the rotation. Moreover, the phase $\phi_{b,\text{cw}}$ can significantly change the transmission windows with a period 2π. To give more details, in **Figures 5C,D** we plot the profiles of T_R and T_L changing with Δ_c/κ for $\phi_{b,\text{cw}} = \pi$ and $\phi_{b,\text{cw}} = 1.5\pi$. By contrast, one finds that for $\phi_{b,\text{cw}} = \pi$, the CW modes decouple to the waveguide corresponding to an optical dark state with $T_R = 1$, while the CCW modes are excited with a transmission dip in T_L. For $\phi_{b,\text{cw}} = 1.5\pi$, strong coupling with a double-dip-type curve in T_L can be realized. The photon nonreciprocal transmission behavior is observed due to the Sagnac effects and the interference effects among multiple coupling points. Note that for $\phi_{b,\text{cw}} = \pi$, similar results are obtained by tuning the phase $\phi_{a,\text{cw}}$.

In **Figures 6A,B**, we plot the transmission rates T_R and T_L versus the detuning Δ_c/κ for different J_b. For $J_b = 10\kappa$, the transmission spectra display an asymmetric four-dips structure. When decreasing J_b, the transmission dips can be suppressed. Moreover, T_L is always larger (smaller) than T_R in the region of $\Delta_c < 0$ ($\Delta_c > 0$). In order to describe the nonreciprocity clearly, we define the isolation ratio as

$$\mathcal{I}\,(\text{dB}) = -10 \times \log_{10}\frac{T_L}{T_R}. \tag{27}$$

In **Figure 7**, the isolation ratio $\mathcal{I}$ changing with the detuning Δ_c/κ and the coupling strength J_b is plotted. It shows that for $J_b = 0$ the ratio achieves $\mathcal{I} \approx 10$ dB ($\mathcal{I} \approx -5$ dB) when fixing $\Delta_c = 11\kappa$ ($\Delta_c = -11.5\kappa$). As we increase J_b, a larger mode splitting for $\Delta_c > 0$ is observed. For $J_b = 10\kappa$, the ratio reaches $\mathcal{I} \approx 17$ dB when Δ_c is set as 15κ. In this case, the photons coming from the left side are blocked, which implies a directional photon transfer between different coupling points. Therefore, the nonreciprocal transmission behavior is also controlled by adjusting the coupling strengths between the CW and CCW modes and the detuning Δ_c.

4 CONCLUSION

In conclusion, we have explored the photon emission and transport properties of spinning resonators coupled to a meandering waveguide at multiple coupling points. We demonstrate that the accumulated phases between multiple coupling points for photons propagating in CW and CCW directions are different. Both "giant-atoms" induced interference effects and mode frequency shifts led by the Sagnac effect dramatically modify photon transport properties. The emission direction and rates can be tuned by changing the spinning speed or number of coupling points. Moreover, the complete photon transmission over the whole optical frequency band led by destructive interference is observed, when photons coming from the right hand of the waveguide. This nonreciprocal phenomenon is very different from that observed in other optical systems. We have also studied the extended two-cavity system. The nonreciprocal photon transmission is controlled by changing the phases among adjacent coupling points or coupling strengths between the CW and CCW modes. By extending our proposal to multiple cavities interacting with multiple points, one can implement a multi-node chiral quantum network. In experiment, such a system with a spinning spherical resonator coupling to a stationary taper has been realized, where the angular speed is about 6.6 kHz [51]. The silica nanoparticle rotating with frequency exceeding 1 GHz has also been reported [62]. Therefore, we believe our theoretical proposals can be realized under current experimental approach. Those results in our paper provide a novel way to engineer rotatable nonreciprocal optical devices, which can be exploited for the realization of large-scale quantum networks and quantum information processing.

DATA AVAILABILITY STATEMENT

The original contributions presented in the study are included in the article/**Supplementary Material**, further inquiries can be directed to the corresponding author.

AUTHOR CONTRIBUTIONS

XW contributed to conception. WL performed the numerical simulations and produced the first draft. All authors contributed to manuscript revision, read, and approved the submitted version.

FUNDING

WL was supported by the Natural Science Foundation of Henan Province (No. 222300420233). XW was supported by the National Natural Science Foundation of China (NSFC) (Nos. 12174303 and 11804270) and the China Postdoctoral Science Foundation (No. 2018M631136).

SUPPLEMENTARY MATERIAL

The Supplementary Material for this article can be found online at: https://www.frontiersin.org/articles/10.3389/fphy.2022.894115/full#supplementary-material

Supplementary Figure S1 | The Sagnac-Fizeu shift Δ_F as a function of the spinning angular velocity Ω for the CW (red line) and CCW (blue line) mode. Other related parameters are Λ = 1550~nm, R = 4.73~nm, and n = 1.4.

REFERENCES

1. Zheng H, Gauthier DJ, Baranger HU. Waveguide-QED-based Photonic Quantum Computation. *Phys Rev Lett* (2013) 111:090502. doi:10.1103/PhysRevLett.111.090502
2. Liao Z, Zeng X, Nha H, Zubairy MS. Photon Transport in a One-Dimensional Nanophotonic Waveguide QED System. *Phys Scr* (2016) 91:063004. doi:10.1088/0031-8949/91/6/063004
3. Roy D, Wilson CM, Firstenberg O. Colloquium : Strongly Interacting Photons in One-Dimensional Continuum. *Rev Mod Phys* (2017) 89:021001. doi:10.1103/RevModPhys.89.021001
4. Akimov AV, Mukherjee A, Yu CL, Chang DE, Zibrov AS, Hemmer PR, et al. Generation of Single Optical Plasmons in Metallic Nanowires Coupled to Quantum Dots. *Nature* (2007) 450:402–6. doi:10.1038/nature06230
5. Vetsch E, Reitz D, Sagué G, Schmidt R, Dawkins ST, Rauschenbeutel A. Optical Interface Created by Laser-Cooled Atoms Trapped in the Evanescent Field Surrounding an Optical Nanofiber. *Phys Rev Lett* (2010) 104:203603. doi:10.1103/PhysRevLett.104.203603
6. Goban A, Hung C-L, Yu S-P, Hood JD, Muniz JA, Lee JH, et al. Atom-light Interactions in Photonic Crystals. *Nat Commun* (2014) 5:1–9. doi:10.1038/ncomms4808
7. Goban A, Hung C-L, Hood JD, Yu S-P, Muniz JA, Painter O, et al. Superradiance for Atoms Trapped along a Photonic crystal Waveguide. *Phys Rev Lett* (2015) 115:063601. doi:10.1103/PhysRevLett.115.063601
8. Corzo NV, Gouraud B, Chandra A, Goban A, Sheremet AS, Kupriyanov DV, et al. Large Bragg Reflection from One-Dimensional Chains of Trapped Atoms Near a Nanoscale Waveguide. *Phys Rev Lett* (2016) 117:133603. doi:10.1103/PhysRevLett.117.133603
9. Astafiev O, Zagoskin AM, Abdumalikov AA, Jr, Pashkin YA, Yamamoto T, Inomata K, et al. Resonance Fluorescence of a Single Artificial Atom. *Science* (2010) 327:840–3. doi:10.1126/science.1181918
10. Van Loo AF, Fedorov A, Lalumière K, Sanders BC, Blais A, Wallraff A. Photon-mediated Interactions between Distant Artificial Atoms. *Science* (2013) 342:1494–6. doi:10.1126/science.1244324
11. Hoi I-C, Palomaki T, Lindkvist J, Johansson G, Delsing P, Wilson CM. Generation of Nonclassical Microwave States Using an Artificial Atom in 1D Open Space. *Phys Rev Lett* (2012) 108:263601. doi:10.1103/PhysRevLett.108.263601
12. Shen JT, Fan S. Coherent Photon Transport from Spontaneous Emission in One-Dimensional Waveguides. *Opt Lett* (2005) 30:2001. doi:10.1364/OL.30.002001
13. Zhou L, Gong ZR, Liu Y-x., Sun CP, Nori F. Controllable Scattering of a Single Photon inside a One-Dimensional Resonator Waveguide. *Phys Rev Lett* (2008) 101:100501. doi:10.1103/PhysRevLett.101.100501
14. Witthaut D, Sørensen AS. Photon Scattering by a Three-Level Emitter in a One-Dimensional Waveguide. *New J Phys* (2010) 12:043052. doi:10.1088/1367-2630/12/4/043052
15. Huang J-F, Shi T, Sun CP, Nori F Controlling Single-Photon Transport in Waveguides with Finite Cross Section. *Phys Rev A* (2013) 88:013836. doi:10.1103/PhysRevA.88.013836
16. Liao Z, Nha H, Zubairy MS. Dynamical Theory of Single-Photon Transport in a One-Dimensional Waveguide Coupled to Identical and Nonidentical Emitters. *Phys Rev A* (2016) 94:053842. doi:10.1103/PhysRevA.94.053842
17. Xiao Y-F, Li M, Liu Y-C, Li Y, Sun X, Gong Q. Asymmetric Fano Resonance Analysis in Indirectly Coupled Microresonators. *Phys Rev A* (2010) 82:065804. doi:10.1103/PhysRevA.82.065804
18. Li B-B, Xiao Y-F, Zou C-L, Jiang X-F, Liu Y-C, Sun F-W, et al. Experimental Controlling of Fano Resonance in Indirectly Coupled Whispering-Gallery Microresonators. *Appl Phys Lett* (2012) 100:021108. doi:10.1063/1.3675571
19. Sinha K, Meystre P, Goldschmidt EA, Fatemi FK, Rolston SL, Solano P. Non-Markovian Collective Emission from Macroscopically Separated Emitters. *Phys Rev Lett* (2020) 124:043603. doi:10.1103/PhysRevLett.124.043603
20. Yu Y, Ma F, Luo X-Y, Jing B, Sun P-F, Fang R-Z, et al. Entanglement of Two Quantum Memories via Fibres over Dozens of Kilometres. *Nature* (2020) 578:240–5. doi:10.1038/s41586-020-1976-7
21. Mitsch R, Sayrin C, Albrecht B, Schneeweiss P, Rauschenbeutel A. Quantum State-Controlled Directional Spontaneous Emission of Photons into a Nanophotonic Waveguide. *Nat Commun* (2014) 5:1–5. doi:10.1038/ncomms6713
22. Le Feber B, Rotenberg N, Kuipers L. Nanophotonic Control of Circular Dipole Emission. *Nat Commun* (2015) 6:1–6. doi:10.1038/ncomms7695
23. Frisk Kockum A, Delsing P, Johansson G. Designing Frequency-dependent Relaxation Rates and Lamb Shifts for a Giant Artificial Atom. *Phys Rev A* (2014) 90:013837. doi:10.1103/PhysRevA.90.013837
24. Guo L, Grimsmo A, Kockum AF, Pletyukhov M, Johansson G. Giant Acoustic Atom: a Single Quantum System with a Deterministic Time Delay. *Phys Rev A* (2017) 95:053821. doi:10.1103/PhysRevA.95.053821
25. Kockum AF, Johansson G, Nori F. Decoherence-free Interaction between Giant Atoms in Waveguide Quantum Electrodynamics. *Phys Rev Lett* (2018) 120:140404. doi:10.1103/PhysRevLett.120.140404
26. Kannan B, Ruckriegel MJ, Campbell DL, Frisk Kockum A, Braumüller J, Kim DK, et al. Waveguide Quantum Electrodynamics with Superconducting Artificial Giant Atoms. *Nature* (2020) 583:775–9. doi:10.1038/s41586-020-2529-9
27. Zhao W, Wang Z. Single-photon Scattering and Bound States in an Atom-Waveguide System with Two or Multiple Coupling Points. *Phys Rev A* (2020) 101:053855. doi:10.1103/PhysRevA.101.053855
28. Frisk Kockum A. Quantum Optics with Giant Atoms-The First Five Years. In: *International Symposium on Mathematics, Quantum Theory, and Cryptography*. Singapore: Springer (2021). p. 125–46. doi:10.1007/978-981-15-5191-8_12
29. Yu H, Wang Z, Wu J-H. Entanglement Preparation and Nonreciprocal Excitation Evolution in Giant Atoms by Controllable Dissipation and Coupling. *Phys Rev A* (2021) 104:013720. doi:10.1103/PhysRevA.104.013720
30. Du L, Chen Y-T, Li Y. Nonreciprocal Frequency Conversion with Chiral Λ -type Atoms. *Phys Rev Res* (2021) 3:043226. doi:10.1103/PhysRevResearch.3.043226
31. Du L, Cai M-R, Wu J-H, Wang Z, Li Y. Single-photon Nonreciprocal Excitation Transfer with Non-markovian Retarded Effects. *Phys Rev A* (2021) 103:053701. doi:10.1103/PhysRevA.103.053701
32. Wang X, Liu T, Kockum AF, Li H-R, Nori F. Tunable Chiral Bound States with Giant Atoms. *Phys Rev Lett* (2021) 126:043602. doi:10.1103/PhysRevLett.126.043602
33. Wang X, Li HR. Chiral Quantum Network with Giant Atoms (2021). *arXiv preprint arXiv:2106.13187*.
34. Soro A, Kockum AF. Chiral Quantum Optics with Giant Atoms. *Phys Rev A* (2022) 105:023712. doi:10.1103/PhysRevA.105.023712
35. Du L, Chen YT, Zhang Y, Li Y. Giant Atoms with Time-dependent Couplings (2022). *arXiv preprint arXiv:2201.12575*.
36. Gustafsson MV, Aref T, Kockum AF, Ekström MK, Johansson G, Delsing P. Propagating Phonons Coupled to an Artificial Atom. *Science* (2014) 346:207–11. doi:10.1126/science.1257219
37. Manenti R, Kockum AF, Patterson A, Behrle T, Rahamim J, Tancredi G, et al. Circuit Quantum Acoustodynamics with Surface Acoustic Waves. *Nat Commun* (2017) 8:1–6. doi:10.1038/s41467-017-01063-9
38. Andersson G, Suri B, Guo L, Aref T, Delsing P. Non-exponential Decay of a Giant Artificial Atom. *Nat Phys* (2019) 15:1123–7. doi:10.1038/s41567-019-0605-6
39. Goto T, Dorofeenko AV, Merzlikin AM, Baryshev AV, Vinogradov AP, Inoue M, et al. Optical Tamm States in One-Dimensional Magnetophotonic Structures. *Phys Rev Lett* (2008) 101:113902. doi:10.1103/PhysRevLett.101.113902
40. Khanikaev AB, Mousavi SH, Shvets G, Kivshar YS. One-way Extraordinary Optical Transmission and Nonreciprocal Spoof Plasmons. *Phys Rev Lett* (2010) 105:126804. doi:10.1103/PhysRevLett.105.126804
41. Fan L, Wang J, Varghese LT, Shen H, Niu B, Xuan Y, et al. An All-Silicon Passive Optical Diode. *Science* (2012) 335:447–50. doi:10.1126/science.1214383
42. Cao Q-T, Wang H, Dong C-H, Jing H, Liu R-S, Chen X, et al. Experimental Demonstration of Spontaneous Chirality in a Nonlinear Microresonator. *Phys Rev Lett* (2017) 118:033901. doi:10.1103/PhysRevLett.118.033901
43. Lira H, Yu Z, Fan S, Lipson M. Electrically Driven Nonreciprocity Induced by Interband Photonic Transition on a Silicon Chip. *Phys Rev Lett* (2012) 109:033901. doi:10.1103/PhysRevLett.109.033901

44. Estep NA, Sounas DL, Soric J, Alù A. Magnetic-free Non-reciprocity and Isolation Based on Parametrically Modulated Coupled-Resonator Loops. *Nat Phys* (2014) 10:923–7. doi:10.1038/nphys3134
45. Sounas DL, Alù A. Non-reciprocal Photonics Based on Time Modulation. *Nat Photon* (2017) 11:774–83. doi:10.1038/s41566-017-0051-x
46. Lu X, Cao W, Yi W, Shen H, Xiao Y. Nonreciprocity and Quantum Correlations of Light Transport in Hot Atoms via Reservoir Engineering. *Phys Rev Lett* (2021) 126:223603. doi:10.1103/PhysRevLett.126.223603
47. Jing H, Lü H, Özdemir SK, Carmon T, Nori F. Nanoparticle Sensing with a Spinning Resonator. *Optica* (2018) 5:1424–30. doi:10.1364/OPTICA.5.001424
48. Li B, Huang R, Xu X, Miranowicz A, Jing H. Nonreciprocal Unconventional Photon Blockade in a Spinning Optomechanical System. *Photon Res* (2019) 7: 630–41. doi:10.1364/PRJ.7.000630
49. Huang R, Miranowicz A, Liao J-Q, Nori F, Jing H. Nonreciprocal Photon Blockade. *Phys Rev Lett* (2018) 121:153601. doi:10.1103/PhysRevLett.121.153601
50. Jiao Y-F, Zhang S-D, Zhang Y-L, Miranowicz A, Kuang L-M, Jing H. Nonreciprocal Optomechanical Entanglement against Backscattering Losses. *Phys Rev Lett* (2020) 125:143605. doi:10.1103/PhysRevLett.125.143605
51. Maayani S, Dahan R, Kligerman Y, Moses E, Hassan AU, Jing H, et al. Flying Couplers above Spinning Resonators Generate Irreversible Refraction. *Nature* (2018) 558:569–72. doi:10.1038/s41586-018-0245-5
52. Fang Y-LL, Baranger HU Waveguide QED: Power Spectra and Correlations of Two Photons Scattered off Multiple Distant Qubits and a Mirror. *Phys Rev A* (2015) 91:053845. doi:10.1103/PhysRevA.91.053845
53. Zhu J, Özdemir SK, Xiao Y-F, Li L, He L, Chen D-R, et al. On-chip Single Nanoparticle Detection and Sizing by Mode Splitting in an Ultrahigh-Q Microresonator. *Nat Photon* (2010) 4:46–9. doi:10.1038/nphoton.2009.237
54. Özdemir ŞK, Zhu J, Yang X, Peng B, Yilmaz H, He L, et al. Highly Sensitive Detection of Nanoparticles with a Self-Referenced and Self-Heterodyned Whispering-Gallery Raman Microlaser. *Proc Natl Acad Sci U.S.A* (2014) 111:E3836–E3844. doi:10.1073/pnas.1408283111
55. Malykin GB. The Sagnac Effect: Correct and Incorrect Explanations. *Phys.-Usp.* (2000) 43:1229–52. doi:10.1070/pu2000v043n12abeh000830
56. Fermi E. Quantum Theory of Radiation. *Rev Mod Phys* (1932) 4:87–132. doi:10.1103/RevModPhys.4.87
57. Xiao Y-F, Gaddam V, Yang L. Coupled Optical Microcavities: an Enhanced Refractometric Sensing Configuration. *Opt Express* (2008) 16:12538–43. doi:10.1364/OE.16.012538
58. Xu S, Fan S. Fano Interference in Two-Photon Transport. *Phys Rev A* (2016) 94:043826. doi:10.1103/PhysRevA.94.043826
59. Du L, Wang Z, Li Y. Controllable Optical Response and Tunable Sensing Based on Self Interference in Waveguide QED Systems. *Opt Express* (2021) 29: 3038–54. doi:10.1364/OE.412996
60. Cai QY, Jia WZ. Coherent Single-Photon Scattering Spectra for a Giant-Atom Waveguide-QED System beyond the Dipole Approximation. *Phys Rev A* (2021) 104:033710. doi:10.1103/PhysRevA.104.033710
61. Feng SL, Jia WZ. Manipulating Single-Photon Transport in a Waveguide-QED Structure Containing Two Giant Atoms. *Phys Rev A* (2021) 104:063712. doi:10.1103/PhysRevA.104.063712
62. Reimann R, Doderer M, Hebestreit E, Diehl R, Frimmer M, Windey D, et al. GHz Rotation of an Optically Trapped Nanoparticle in Vacuum. *Phys Rev Lett* (2018) 121:033602. doi:10.1103/PhysRevLett.121.033602

Conflict of Interest: The authors declare that the research was conducted in the absence of any commercial or financial relationships that could be construed as a potential conflict of interest.